Hybridization, superexchange, and competing magnetoelastic interactions in TiOBr

Macovez, Roberto; Luzon, Javier; Schiessling, Joachim; Sadoc, Aymeric; Kjeldgaard, Lisbeth; van Smaalen, Sander; Fausti, Daniele; van Loosdrecht, Paul H. M.; Broer, Ria; Rudolf, Petra

Published in:
Physical Review. B: Condensed Matter and Materials Physics

DOI:
10.1103/PhysRevB.76.205111

Publication date:
2007

Hybridization, superexchange, and competing magnetoelastic interactions in TiOBr

Roberto Macovez,[1] Javier Luzon,[1] Joachim Schiessling,[2] Aymeric Sadoc,[1] Lisbeth Kjeldgaard,[3] Sander van Smaalen,[4] Daniele Fausti,[1] Paul H. M. van Loosdrecht,[1] Ria Broer,[1] and Petra Rudolf[1]

[1]*Zernike Institute for Advanced Materials, University of Groningen, Nijenborgh 4, NL-9747AG Groningen, The Netherlands*

[2]*Department of Physics, Uppsala University, Box 530, SE-75121 Uppsala, Sweden*

[3]*Max-lab, University of Lund, Box 118, SE-22100 Lund, Sweden*

[4]*Laboratory of Crystallography, University of Bayreuth, D-95440 Bayreuth, Germany*

(Received 23 June 2007; revised manuscript received 21 September 2007; published 20 November 2007)

A crystalline sample of TiOBr is probed at room temperature by a combination of electron spectroscopies and the results are compared to theoretical embedded-cluster calculations. Resonant photoemission of the valence band confirms that the lowest binding energy feature arises from the singly occupied Ti 3*d* orbital. The polarization dependence of this orbital in nonresonant photoemission is consistent with the expected dominant $d_{y^2-z^2}$ character. The analysis of the Ti $L_{2,3}$ x-ray absorption spectra confirms the complete splitting of the Ti 3*d* shell. X-ray absorption and resonant photoemission at the O 1*s* edge provide direct evidence for hybridization between the transition metal orbitals and the O 2*p* levels, which leads to superexchange interactions between the Ti ions. The existence of a mixing of O and Ti states and of strong superexchange interactions is supported by calculations of the ground-state electronic and magnetic properties. The calculated superexchange interchain interaction is one fifth in strength of the total magnetic coupling along the chain, and is antiferromagnetic in character. This O-mediated interchain interaction is frustrated in the room temperature phase of TiOBr and thus couples strongly to distortions of the soft lattice. The competition between the interchain magnetoelastic coupling and the spin-Peierls interaction might be at the origin of the complex TiO*X* phase diagram.

DOI: 10.1103/PhysRevB.76.205111 PACS number(s): 71.27.+a, 71.70.−d, 78.70.Dm, 79.60.−i

I. INTRODUCTION

Titanium oxyhalides (chemical formula TiO*X* with *X* =Cl, Br) have attracted much attention in the past four years due to their quasi-one-dimensional (1D) magnetic character[1] and because they represent the electron analog ($3d^1$) of the cuprate oxides ($3d^9$). The TiO*X* crystal structure consists of buckled TiO bilayers stacked along the crystallographic **c** axis and separated from one another by two halogen planes. Each bilayer contains alternating Ti and O arrays oriented parallel to the **b** axis.[2,3] The nominal valence charges are X^-, O^{2-}, and Ti^{3+} (electronic configuration $3d^1$). The halogens are expected to have almost pure ionic character, while the ionic bonding inside the TiO bilayers is expected to have a partial covalent character.

TiOBr and TiOCl have a strikingly similar phase diagram. At high temperature they crystallize in the FeOCl structure type[2,3] with each Ti ion surrounded by a heavily distorted O_4X_2 octahedron. While band theory predicts a metallic ground state, TiO*X* is an insulator. It is believed that the ligand field of C_{2v} symmetry lifts completely the degeneracy of the Ti 3*d* shell, and that the ground state orbital, which is filled by only one electron, has lobes pointing along **b** and **c**.[1,4] Due to the large Coulomb repulsion at the Ti site, the *d* electron in the ground state acts to a large degree as a localized spin.

Direct overlap of adjacent *d* orbitals only occurs along **b**, and the resulting 1D exchange interaction leads at room temperature to the formation of antiferromagnetic spin chains.[1,5] As the temperature is lowered, TiO*X* displays a second order transition to an incommensurate phase at T_{c2}, followed, at a lower critical temperature T_{c1}, by a first order transition to a spin Peierls phase with doubling of the unit cell along **b**. The transition temperatures are T_{c1}=27 K (67 K) and T_{c2}=47 K (91 K) for TiOBr (TiOCl).[1,6,7] The phase diagram of TiO*X* is at odds with the conventional spin-Peierls scenario where only one (second order) transition is expected.

The origin of the unconventional spin-Peierls behavior of TiO*X* is debated. Early studies speculated that orbital fluctuations might play a role in the high temperature phase, suggesting that phonon-induced orbital fluctuations might be present at high temperatures.[4,8–10] This scenario has been, however, refuted by other studies. Density functional calculations[4] in the local density approximation with a Hubbard-like correction (LDA+U) as well as a more recent cluster computation[11] gave an energy separation of 0.3 eV between the ground state orbital and the first excited Ti 3*d* state, which is too high for mixed-orbital ordering to occur. The lack of a dynamical Jahn-Teller admixture of higher lying *d* levels in the ground state has been confirmed experimentally.[12–14] The microscopic mechanism responsible for the complex phase diagram of TiO*X* is not fully understood.[13,15] A detailed knowledge of the ground state above T_{c2} is helpful to clarify this issue.

II. METHODS

To investigate the electronic structure of TiOBr we performed photoemission (PES), resonant photoemission, and x-ray absorption (XAS) spectroscopy measurements, accompanied by *ab initio* embedded-cluster calculations of the electronic structure and of the relevant magnetic interactions in the room-temperature phase.

A **c**-oriented TiOBr crystal was grown by chemical vapor transport[3,16] and its crystallinity checked by x-ray diffraction. Experiments were performed at the surface branch of beam-

line I-511 (Ref. 17) of the MAXlab-II synchrotron radiation facility. The sample was introduced in the entry lock of the experimental chamber and cleaved there in an inert nitrogen atmosphere. The loadlock was then pumped down and the sample was transferred to the experimental chamber (base pressure 1×10^{-10} mbar). The light polarization could be varied from parallel to normal with respect to the sample surface without modifying the photoelectron detection geometry, which could be chosen to be normal with respect to the sample (7° from the surface normal) or grazing (70° from the surface normal). The analyzer acceptance angle was ±6°. The XAS spectra were acquired by varying the photon energy across the Ti $L_{2,3}$ and O K absorption edges and measuring the induced Auger decay or the total electron yield. Resonant photoemission of the valence band states was performed at the same photon energies. The experimental resolution was better than 0.1 eV for both PES and XAS. Special precautions were taken to avoid charging effects during the measurements, which easily occurred due to the strongly insulating character of TiOBr. The sample was glued with silver paste onto a metallic substrate to ensure the best possible grounding. All measurements were performed at room temperature, and the photon flux was lowered until neither binding energy shifts nor broadening of the photoemission features could be detected in the valence band spectrum.

The theoretical study was performed using the embedded cluster approach. To approximate the *N*-electron wave function, the restricted active space self-consistent field (RASSCF) method was used. This method allows a treatment of electron correlation in which a restricted number of electrons is correlated whereas all other electrons are considered to be in doubly occupied orbitals (inactive space). This restricted space is divided in three orbital-specific spaces starting from RAS1 for which orbitals contain a chosen maximum number of holes and ending with RAS3 where we consider orbitals containing a maximum number of electrons. The RAS2 orbital space contains all electrons that are not in RAS1, RAS3, or inactive orbitals. The configuration interaction (CI) expansion of the wave function includes all possible distributions of the electrons within the restrictions mentioned above. Using only the RAS2 space (i.e., if the RAS1 and RAS3 contain no orbitals) yields a conventional complete active space self-consistent field (CASSCF) calculation. In a RASSCF or CASSCF calculation not only the CI expansion coefficients, but also the orbitals are optimized. Often a common set of orbitals is optimized for a weighted average of a number of similar, closely lying states.

The ground state electronic structure of an embedded $[TiO_4Br_2]^{7-}$ cluster was first investigated using only the RAS2 space containing one electron in five orbitals [corresponding to a CAS(1,5)SCF calculation]. The cluster was surrounded by eight Ti^{3+} represented by total ion potentials[18] in order to account for the electrostatic interaction between the cluster atoms and the shell of first neighbor atoms, and further embedded in a field of point charges fitted to reproduce the Madelung field due to the rest of the crystal. The crystal lattice is taken from Ref. 2. The orbitals in the cluster region were derived from a $(21s15p10d6f4g)$ primitive basis set for the titanium and a $(14s9p4d3f)$ primitive basis set for the oxygen ions. Following the atomic natural orbital (ANO) contraction of Widmark and coworkers,[19,20] we used a $(14s9p4d3f)$ basis for Ti and a $(4s3p)$ basis for O. These are the so-called ANO-L bases as implemented in the MOLCAS quantum chemistry package.[21] For the Br atoms, an effective core potential (ECP) with a valence basis set from Dolg[22] was employed. To obtain the ground state electron distribution a small active space consisting of five orbitals of mainly Ti $3d$ character is sufficient, as dynamical electron correlation effects are expected to be small for the charge distribution of this state with one single $3d$ electron.

Theoretical modeling of the O $1s$ and Ti $2p$ XAS spectra was performed. To simulate a hole in one of the four oxygen $1s$ orbitals of a TiO_4Br_2 cluster, the nuclear charge of that atom was increased from 8 to 9. In addition, an electron was added to the cluster and the energies of the $3d^2$ manifold were obtained from CAS(2,5)SCF calculations. This simple procedure was repeated for each oxygen ligand in order to gain an insight in the origin of the lowest-energy peaks in an O $1s$ XAS spectrum. For each oxygen hole the final state wave functions were obtained from two average RASSCF calculations (one for the spin-singlet and one for the spin-triplet states of the $3d^2$ manifold). A more advanced method is required to simulate the Ti $2p$ spectrum because in this case it is necessary to include relativistic effects, in particular the spin-orbit coupling. Initial $(2p^6\ 3d^1)$ and final $(2p^5\ 3d^2)$ states without spin-orbit coupling effects were initially obtained from RASSCF calculations using the same embedded cluster and basis sets as for the computation of the ground state. The RAS2 space used for this computation contains ten orbitals (5 Ti $3d$+5 Ti $3d'$), where the five $3d'$ orbitals are added to allow for a proper treatment of dynamic electronic correlation. For the computation of the final states the three Ti $2p$ orbitals were constrained to be in the RAS3 space, with a maximum of five electrons. Due to the large number of final-state wave functions to be computed (75 for $S=M_s=1/2$ states and 30 for $S=3/2$ states), these were obtained from four average RASSCF calculations, one for each irreducible representation of the C_{2v} point group. The resulting initial and final state wave functions were then used as input for a RASSCF state interaction (RASSI) computation performed in order to include the spin-orbit coupling and to compute the absorption intensity for the ensuing 270 final absorption lines.[23] The calculated spectrum was broadened with a Gaussian and a Lorentzian function to mimic the instrumental resolution and lifetime broadening. A full width at half maximum of 0.1 eV was used for the Gaussian function to reproduce the experimental resolution. The Lorentzian width was set to 0.2 eV, which is a typical value of lifetime broadening for $2p$ core levels in $3d$ transition metal oxides.[24]

The magnetic interactions were computed within the density functional theory (DFT) broken-symmetry approach using the scheme proposed by Yamaguchi[25] and the B3LYP exchange-correlation potential[26] with a 6-311G* Gaussian basis set.[27] For the computation of each magnetic interaction, a cluster containing the two interacting Ti ions and their O and Br first neighbors was considered. The next shell of Ti^{3+} ions was simulated by Al^{3+} ECP potentials and the resulting cluster embedded in a distribution of point charges.

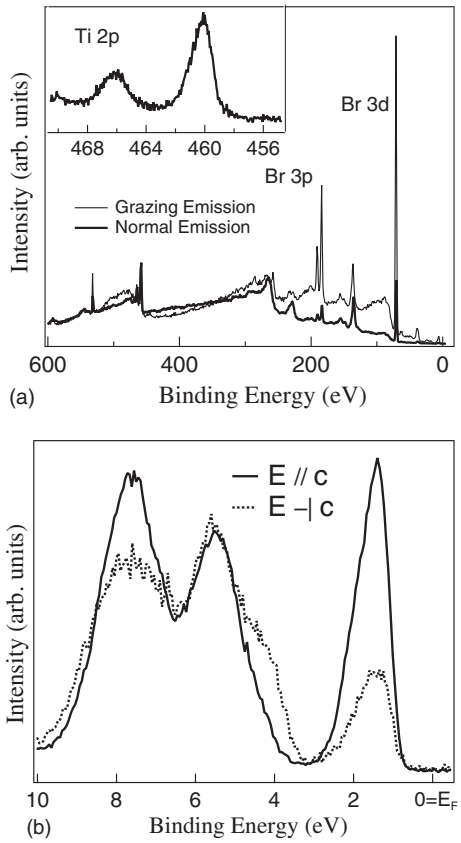

FIG. 1. (a) Overview photoemission spectrum of TiOBr acquired at $h\nu$=650 eV with light polarization orthogonal to **c** in both grazing (GE, thin line) and normal (NE, thick line) emission. The curves are normalized to the background signal at high kinetic energy and at the Fermi level. Inset: Ti 2*p* photoemission spectrum acquired at the same photon energy in normal emission. (b) Normal emission valence band photoemission spectra with $h\nu$=130 eV, normalized to the height of the mainly Br-derived peak at 5.5 eV binding energy (see text). Continuous line: **E** parallel to **c**; dotted line: **E** perpendicular to **c**.

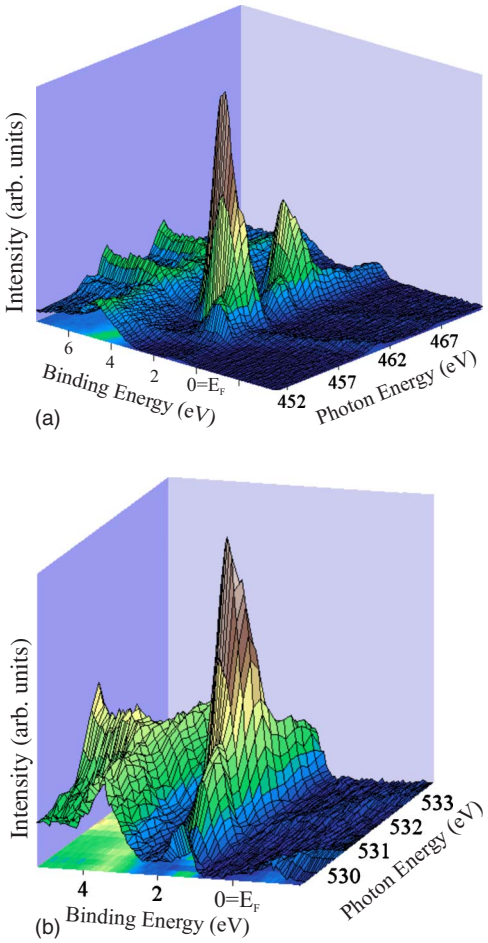

FIG. 2. (Color online) 3D false-color map of the valence band resonant PES spectra at the Ti 2*p* (a) and O 1*s* (b) absorption edges.

III. RESULTS AND DISCUSSION

A. Photoemission and resonant photoemission spectra

Figure 1(a) shows the overview photoemission spectra measured in both emission geometries with 650 eV photon energy and light polarization parallel to the sample surface. The absence of extra peaks other than Br, Ti, and O features establishes that the sample is pure and that the surface is free of adsorbates. Comparison between the two geometries indicates that the crystal is Br terminated, which is expected since the covalently bonded TiO bilayers interact via van der Waals forces, so that cleavage occurs between adjacent halogen planes. The final state spin-orbit splitting of the Ti 2*p* core level is 6 eV, as visible in the inset of Fig. 1(a).

The PES intensity in the valence band region, shown in Fig. 1(b) for the two light polarizations, derives from O 2*p*, Br 4*p*, and Ti 3*d* states. The lowest binding energy feature has mainly Ti character (see below). A preliminary DFT study[28] of the orbital-projected density of states in TiOBr shows that the spectral feature at 8 eV binding energy has mostly O 2*p* character, while the components at intermediate binding energies have a dominant Br 4*p* character. Similar results were obtained in recent DFT calculations using the generalized gradient approximation including the on-site Hubbard U.[29] Our valence band spectra display the same structure as the angle-resolved spectra measured on TiOCl and TiOBr.[12,29] The Ti-derived feature at lowest binding energy is well-separated from the rest of the spectrum in both systems, though the separation is smaller in the TiOBr case due to the larger unit cell,[29] and has a similar width in both cases (roughly 2.5 eV).

Figure 2 shows the resonant valence band photoemission spectra acquired at various photon energies across the Ti 2*p* and O 1*s* absorption edges. In the spectra acquired at the Ti 2*p* edge [Fig. 2(a)] a large resonant enhancement of the Ti feature is observed. As a function of the photon energy the intensity of the feature closest to E_F displays two maxima which are 6 eV apart. These correspond to the resonant process involving the two possible spin-orbit states of the Ti 2*p* core hole. It can be seen in Fig. 2(a) that also the intensity of the other valence band features is slightly enhanced across the two thresholds, signaling a partial Ti character of these states as well. The enhancement of the lowest binding energy feature is by far the most important, which confirms that this feature derives mainly from Ti states.

The mainly Ti 3*d*-derived feature displayed a resonant enhancement also when the excitation light was varied across the O 1*s* edge [Fig. 2(b)], though the magnitude of the enhancement was smaller than for the Ti 2*p* edge. The observation of such a resonance indicates that there is a significant admixture of O 2*p* character to the mainly Ti 3*d*-derived band, as will be discussed in more detail in relation to the x-ray absorption spectra. In the resonant photoemission at the O K edge also the states above 3 eV binding energy are enhanced, especially those at highest binding energy, which is in agreement with their dominant oxygen character.[29] A small peak appears above the Ti 3*d* states for photon energies right above each absorption edge. The binding energy of the features scales linearly with the photon energy, which shows that they originate from the Auger decay of the Ti 2*p* and O 1*s* core hole, respectively.

As visible in Fig. 1(b), the intensity ratio between the Ti 3*d* states and the O- and Br-derived density of states is higher when the light polarization is parallel to **c**. This reflects the fact that the ground state orbital has mainly $d_{y^2-z^2}$ character (we use the convention of Ref. 13 for which $x \| \mathbf{a}$, $y \| \mathbf{b}$, and $z \| \mathbf{c}$). In normal emission the directions of the detected photoelectrons form a cone around the **c** axis. Due to polarization selection rules, electrons occupying an orbital of even parity with respect to a plane containing the crystallographic direction **c** (such as the $d_{y^2-z^2}$ orbital) can be photoemitted in that direction only if the polarization of the incident light is parallel to **c**.[30] The nonzero signal recorded with light polarization perpendicular to **c** is here mainly due to the geometry of the experiment: the sample had to be tilted slightly (less than 10°) toward the impinging light (the light incidence cannot be perfectly grazing), which implied a similar deviation of the detection direction from the **c** axis. A nonvanishing Ti 3*d* signal with light polarization along **a** was observed also in TiOCl and attributed there to a possible sample misalignment and/or the effect of symmetry-breaking phonons.[12]

We note that the Br- and O-derived features also display a dependence on polarization [Fig. 1(b)]. The shoulder at 4 eV binding energy visible in the spectrum with light polarization in the **ab** plane, mainly Br-derived, is absent in the spectrum taken with the other light polarization. This polarization dependence is in line with the large dispersion of the O and Br valence band states observed in the angle-resolved PES study on TiOBr.[29]

B. Electronic structure calculations of the ground state and excited $3d^1$ states

Our CASSCF cluster study of the valence electronic structure confirms the results of Ref. 11 in that the ground state has one electron in a Ti $3d_{y^2-z^2}$ orbital with some O 2*p* character mixed in. The ground-state singly occupied orbital is shown in Fig. 3. The largest lobes are observed around the central (Ti) atom, confirming the dominant Ti 3*d* character. The contribution to the ground state of oxygen orbitals from the nearest-neighbor O atoms lying close to the **bc** plane containing the central Ti atom (labeled O3 and O4 in Fig. 3) is clearly visible. We have also computed the energies of the higher-lying (excited) $3d^1$ orbitals. Four low-lying excited $3d^1$ states exist, with energies 0.34, 0.70, 1.62, and 2.21 eV above the ground state. These values are similar to those found in our previous study.[11] The geometry of these excited states is the same in both TiOCl and TiOBr.[11] Ir-active orbital excitations were observed[13] at 0.5–0.8 eV (1.3–1.6 eV) with **E** parallel to **a** (**b**) in transmittance experiments on TiOBr. The energy windows of these features correspond to the energies of the computed $3d^1$ excited states at 0.70 and 1.61 eV. The interpretation of the ir transmittance dips in TiOBr is the same as for the corresponding TiOCl spectra.[13,31]

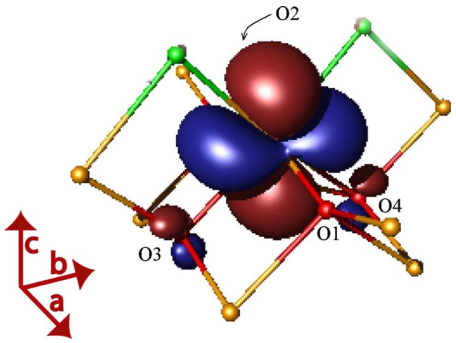

FIG. 3. (Color online) Calculated ground state singly occupied orbital. Besides the main contribution from the Ti 3*d* orbital, visible as the large lobes around the central (Ti) atom of the cluster, some charge density is found at first-neighbor oxygens (marked O1–O4) lying close to the **bc** plane.

Although the 3*d* degeneracy is completely lifted, one can distinguish in the computed $3d^1$ levels three lower-lying t_{2g}-derived and two higher-lying e_g-derived states, separated by an effective crystal field energy splitting of about 1.6 eV. In all five $3d^1$ states (ground state and excited states), the singly occupied orbital shows some hybridization with O 2*p* orbitals. The effect is strongest for the e_g-like orbitals.

C. XAS spectra and calculations for $3d^2$ excited states with a core hole

The O K-edge XAS spectrum of TiOBr is shown in Fig. 4 for the two light polarizations. Since x-ray absorption is an element- and orbital-selective probe, the detection of absorption at the O 1*s* edge is direct evidence for hybridization between the Ti 3*d* and O 2*p* orbitals, as the O 3*s* states lie above the vacuum level, i.e., too high in energy to be observed. On the contrary, we did not measure any absorption at the Br 3*s* or 3*p* core level thresholds, which confirms the ionic character of the Br species in the compound.

As in many other transition metal oxides, the absorption features at the O *K* edge derive from the mixing of the O 1*s* states with the *d* (lower energy) and *s*-*p* (higher energy) orbitals of the transition metal. The signal intensity at the absorption threshold is related to the degree of covalency in the compound, which we have already seen to be non-negligible (Fig. 2). In a quasioctahedral environment, the low energy region of the O 1*s* XAS spectrum usually consists of two peaks, usually associated with the 3*d* t_{2g}-e_g crystal field

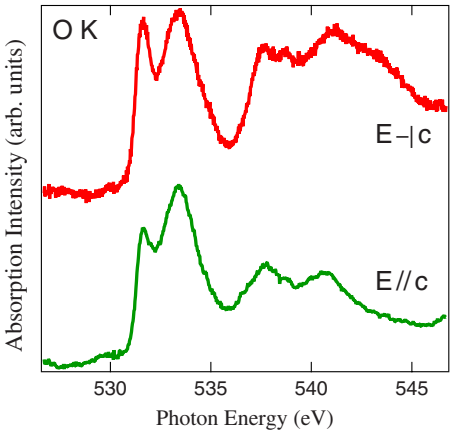

FIG. 4. (Color online) X-ray absorption spectra acquired at the O 1*s* edge, with light polarization orthogonal (⊥) and parallel (∥) to the **c**-axis.

splitting.[32] Two features are indeed observed at low photon energy in the spectra of Fig. 3. However, while in TiO_2 and especially VO_2, which is isoelectronic to TiO*X*, the first of the two hybrid $2p$-$3d$ peaks is more intense than the second,[32,33] the situation is reversed in the O 1*s* XAS spectra of TiOBr.

We can compare the experimental spectra with the result of our computations of the relevant excited states (including the core-hole). There are four oxygen atoms in the unit cell (denoted by O1, O2, O3, and O4 in Fig. 3). The frozen-orbital (ground state) binding energies of the O 1*s* orbital at the four oxygens lie all within 0.1 eV, and similarly we can expect that also excited configurations involving different oxygen atoms similarly do not differ too much in energy. A full calculation involving all possible configurations with a hole at one of the four oxygen ions would be rather tedious and may require larger clusters than those used in the present study. However, as discussed in Sec. II, in order to obtain a reasonable representation of the relative final state energies, it is sufficient to simulate the O 1*s* hole by increasing the nuclear charge on one of the four oxygen nuclei in the unit cell from 8 to 9 and to add an extra electron (representing the excited electron) to the cluster. The spin of the core hole is therefore not considered. However, since the valence electrons are localized mainly on the Ti atom, their spin interaction with the unpaired core spin on the oxygens can be expected to be small. Hence the energies calculated with this approach should be reliable, and furthermore we can limit ourselves to consider the spins of the two open shell electrons in the valence band. These two valence spins can be coupled either to a triplet ($S=1$) or a singlet ($S=0$) state. Both are accessible to XAS, since both can couple with the core spin to form a doublet ($S=1/2$) (which is the spin configuration of the ground state). The results of our calculations are summarized in Table I. Although the Ti site symmetry is not close to octahedral (O_h) symmetry, the final state energies can be well-interpreted with a d^2 Tanabe-Sugano diagram.[34] For each of the four oxygen 1*s* holes the lowest three states have $S=1$ and a $3d$-$t_{2g}{}^2$-like configuration (corresponding to $^3T_1$ in O_h). Triplet states with a $t_{2g}{}^1e_g{}^1$-like configuration ($^3T_{2g}$ and $^3T_{1g}$ in O_h) have energies which are at least 1.3 eV higher than the lowest lying triplet excitations, whereas $t_{2g}{}^2$-like spin-singlet excitations have energies which are 0.8 eV higher than the corresponding triplet configurations (spin-singlet final states involving e_g-like orbitals have even higher energy). Absorption processes in which both electrons are in the higher orbitals in the final configuration (i.e., $t_{2g}{}^0e_g{}^2$-like final states) lie high in energy and contribute a low spectral intensity to the XAS spectrum. The total energy spread of the $t_{2g}{}^2e_g{}^0$ and $t_{2g}{}^1e_g{}^1$ configurations is 4.7 eV. Atomic correlation effects are expected to reduce this interval by about 25% to 3.5 eV, in rather good qualitative agreement with the energy spread of the first two peaks observed in the O K-edge spectra.

TABLE I. Energy differences (in eV) between the lowest-energy spin-triplet $t_{2g}{}^2e_g{}^0$ state and the higher-lying triplet and singlet configurations, calculated using CAS(2,5)SCF on the $3d^2$ manifold of a TiO_4Br_2 cluster with a simulated O1*s* hole. The table summarizes the results obtained for the four possible positions of the core hole. Due to the local symmetry, the oxygen ligands are two by two equivalent and each level shown is twofold degenerate.

Oxygen hole site	O1, O2	O3, O4
ΔE triplet ($t_{2g}{}^1e_g{}^1$)	1.32	1.61
ΔE singlet ($t_{2g}{}^1e_g{}^0$)	0.78	1.28

Based on these results we interpret the first of the two lowest O 1*s* XAS peaks as corresponding to $t_{2g}{}^2$-derived spin-triplet final states and the second peak as being due to a superposition of $t_{2g}{}^2e_g{}^0$-like spin-singlet as well as $t_{2g}{}^1e_g{}^1$-like spin-triplet final states. The calculations do not yield quantitative information on the relative intensities. Nevertheless, the results indicate that only the second peak involves occupation of an e_g-like orbital. In the spectrum acquired with light polarization along **c**, the relative intensity of the first absorption feature is lower than with the orthogonal polarization. This might be related to the fact that the lowest unoccupied d level has d_{xy} symmetry, so that transitions from a $1s^2\ 3d$-$t_{2g}{}^1$ to a $1s^1\ 3d$-$t_{2g}{}^2$ state involving such an orbital are dipole-forbidden when the **E**-vector is parallel to **c**.

Figure 5(a) shows the XAS spectra recorded at the Ti $2p$ edge. The core hole spin-orbit coupling splits the spectra into two replicas, corresponding to the $J=3/2$ (lower photon energy) and $J=1/2$ (higher photon energy) states, with an average separation close to that observed in the photoemission spectrum of the Ti $2p$ core level [inset of Fig. 1(a)]. From statistical arguments owing to the degeneracy of the $2p_{3/2}$ and $2p_{1/2}$ subshells, a L_3/L_2 intensity ratio of 2:1 is expected. While this ratio is in fact observed in the Ti $2p$ PES spectrum, it is not the case for the XAS spectrum. This is a common feature of the $L_{2,3}$ spectrum of many transition metals which originates from a many-electron effect.[35]

The Ti $L_{2,3}$ absorption features arise from $2p^63d^1 \rightarrow 2p^53d^2$ dipole transitions and carry indirect information on the various unoccupied $3d$ states and on their symmetry (orientation). The interaction between the electron in the Ti $3d$ ground state orbital and the second electron which fills

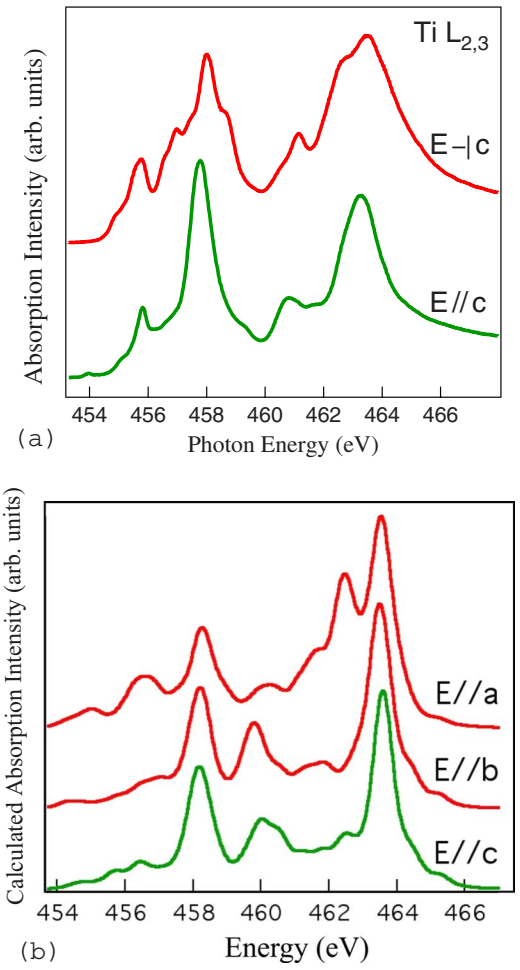

FIG. 5. (Color online) (a) Ti $2p$ x-ray absorption spectrum, acquired with both light polarizations. (b) Simulation of the x-ray absorption spectra assuming light polarization parallel to **a**, **b**, and **c** (from top to bottom).

the unoccupied state in the absorption process, and the coupling between the $2p$ core hole and the $3d$ electrons combine to give rise to a rich multiplet structure. The direct Coulomb interaction is of the order of a few eV, and it is dependent on the symmetry of the empty orbital which is populated in the absorption step. The theoretical Hund's rule energy (the so-called "pairing energy") for two electrons sitting in different t_{2g}-like orbitals is of the order of 1–1.5 eV,[34] and is also orbital-dependent. The spin-orbit interaction in the $3d$ shell and the intersite magnetic exchange are instead much smaller in energy.

The crystal field splitting of the $3d$ shell in TiOBr also enhances the multiplet splitting. The fine structure visible in the lower energy replica of the spectrum with light polarization in the **ab** plane is consistent with the complete splitting of the unoccupied Ti $3d$ levels by the ligand field. The difference in line shape between the two spin-orbit replicas originates as the multiplet lines involved are not equivalent due to the different spin-orbit state of the core hole. Each spin-orbit replica consists of two main groups of features in both light polarizations, of which the group at lower energy is less intense. This is reminiscent of the low-energy line shape of the O $1s$ XAS spectrum, which arises from hybridization with d states. The average energy separation between the two groups of features is roughly 2.5 eV and the total width of each replica is slightly above 4 eV, as found for the O $1s$ XAS spectra.

An interesting feature of Fig. 5(a) is the more pronounced structure observed with light polarization in the **ab** plane. The advantages of XAS over other optical probes are the wider energy range accessible and the less stringent selection rules. While only transitions to the second and third excited $3d^1$ orbitals can be observed in ir transmittance experiments,[13] the XAS spectra contain contributions from transitions to all five d sublevels. We stress, however, that a direct comparison between the two experiments cannot be done due to the different states probed by the two techniques. In particular, XAS involves an intermediate state with a $3d^2$ valence configuration in the presence of a core hole, which strongly modifies the orbitals' symmetry and energy. The absorption features between 456 and 457 eV in the spectrum with light polarization orthogonal to **c**, which are not present in the other polarization, might arise from transitions involving the lowest lying $3d$ level of d_{xy} symmetry, which is unoccupied in the ground state, as discussed also for the O XAS spectra (the corresponding valence band transitions are instead not active in ir).

The theoretical simulation of the Ti $2p$ XAS spectrum is presented in Fig. 5(b). Despite the large number of input states for the RASSI computation, which reduces the accuracy of the calculation, a semiqualitative agreement is observed between the experimental and the theoretical results. In particular, the splitting into two groups of features with an energy separation of around 6 eV is found in the simulated spectra as well, and the line shapes of the experimental and simulated spectrum with **E** parallel to **c** are found to be quite similar, though the energies of the main features do not all correspond exactly. Note, moreover, the relatively more pronounced structure of the calculated spectra with light polarization along **a**, which is reflected in the larger width of the main spectral features around 464 and 458 eV photon energy in the experimental spectrum with light polarization in the **ab** plane. This semiqualitative agreement indicates the validity of our embedded cluster quantum calculations, and further evidences the complete crystal-field splitting of the $3d$ shell.

D. Magnetic interactions

Since our data as well as those of Refs. 12 and 13 exclude the possibility of orbital fluctuations, the existence of an intermediate phase between the room temperature (RT) antiferromagnet and the low temperature spin-Peierls phase, and the unconventional character of the transition at T_{c1}, must be taken as indications that competing orders are at work in titanium oxyhalides. The direct observation of strong hybridization between the Ti and O states, confirmed by our *ab initio* calculations, suggests that oxygen-mediated superexchange might play an important role.

To investigate this we have computed the main magnetic couplings in the RT structure of TiOX: along the chain axis

TABLE II. Calculated magnetic interactions in TiO*X*. The last column reports the values obtained from the analysis of the magnetic susceptibility in the high-temperature phase (see text for details), after Ref. 1 for TiOCl and Ref. 13 for TiOBr.

Compound	J_b (K)	J_{nn} (K)	J_a (K)	J_b (K) (experimental fit)
TiOBr	−250	−47.0	12.0	−375
TiOCl	−353	−40.8	7.4	−660

(J_b), between adjacent nearest-neighbor chains (J_{nn}), and between nonadjacent Ti chains along **a**. The values of these interactions (in units of K) are listed in Table II for both TiOBr and TiOCl.

The coupling J_b is the dominant interaction and is antiferromagnetic in character. The role of the interchain coupling J_{nn}, also antiferromagnetic, is, however, far from marginal, as its intensity is roughly 20% (12%) of the intrachain coupling J_b in TiOBr (TiOCl). The exchange along **a** is instead much weaker, and ferromagnetic in character. The relative strength and character of these three interactions can be explained based on the nature and geometry of the singly occupied orbital. Since there is no admixture in the ground state of d states other than the $d_{y^2-z^2}$ orbital, as previously shown, and because the distance between two Ti ions in adjacent chains is too large to give rise to a significant orbital overlap, the J_{nn} and J_a couplings originate from O-mediated superexchange. The larger admixture of O $2p$ character from oxygens which are coplanar with the ground state $d_{y^2-z^2}$ orbital accounts for the relative strengths of the J_{nn} and J_a interactions.[36]

The J_b coupling has a strong direct-exchange contribution arising from the overlap between occupied $3d$ orbitals on different sites. In addition, the singly occupied orbital shows a delocalization toward the oxygen atoms in the **bc** plane, which enhances the antiferromagnetic J_b magnetic coupling through an O-mediated superexchange mechanism. This is an important result as it shows that the intrachain superexchange is *not* competing against the strong direct exchange in the chain. Instead, it is clear that the interchain coupling J_{nn} is frustrated in the RT structure, where the intrachain coupling establishes parallel antiferromagnetic chains.

From a fit of the magnetic susceptibility of the high-temperature phase of TiOCl with a Bonner-Fisher line shape (assuming i.e., a one-dimensional Heisenberg model), the magnitude of the total magnetic exchange along **b** was determined to be J_b=660 K in this compound.[1] In the TiOBr case, instead, the Bonner-Fisher curve does not provide a good fit to the high-temperature behavior of the susceptibility.[13,37] This testifies to the more important impact of magnetic interactions other than the J_b coupling in TiOBr with respect to TiOCl, which agrees with the fact that our calculated J_{nn}/J_b ratio is almost twice as large in TiOBr as in TiOCl, as reported above. Despite the magnetic susceptibility of the high-temperature phase of TiOBr does not fit a Bonner-Fisher line shape, a J_b=375 K was estimated from the value of the temperature (T_{max}) at which the susceptibility reaches a maximum, taking the nominal ratio of J/T_{max} =0.64 typical of the Bonner-Fisher curve.[13] Our calculated values for J_b are off by a factor less than 2 with respect to the experimental ones. Similar discrepancy may be expected for the computational method used, which is known to provide only estimated values.[38] Estimates of J_b provided by previous theoretical work[4,37] are in somewhat better agreement with the experimental values, but they are based on semiempirical methods which depend on the choice of free parameters (such as U). In addition, these studies do not explicitly take into account magnetic couplings other than along **b**.

Our method yields the correct order of magnitude of the J_b coupling in both compounds, and the ratio between the calculated and experimental estimates[1,13] of J_b is very similar in the two TiO*X* compounds. This indicates that, although the magnitudes of the various J's might be off by a (small) scale factor, our J_{nn}/J_b ratios are reliable estimates of the relative strengths of these interactions. Our calculations indeed confirm the larger deviation of TiOBr from a quasi-1D behavior. We base the following discussion on this result.

We argue that the frustrated J_{nn} superexchange, which couples adjacent Ti chains, plays an important role for the TiO*X* phase diagram. The existence of an interchain interaction was suggested already in Ref. 13. Such interchain coupling was there associated to an electron-lattice mechanism, while our study clearly demonstrates that also a *magnetic* intrachain coupling exists, of superexchange origin. Oxygen-mediated superexchange between transition metal ions is considered to be an important ingredient of the physics of many transition metal oxides, including the high-T_c cuprate superconductors and notably in $CuGeO_3$, the only other example of inorganic spin-Peierls system known so far besides the titanium oxyhalides.[39] A magnetic nature of the interaction competing with the intrachain exchange is also suggested by the reported decrease in T_{c1} in the presence of a magnetic field applied along **b**.[15]

It should be stressed that the transitions observed in the TiO*X* compounds have a magnetoelastic (rather than simply magnetic) origin, and that a proper description of the system must consider the full spin-lattice couplings. Each exchange interaction depends in a sensitive way on the interatomic distances and bond angles with the linking oxygens, and is therefore coupled to the distortion of the rather soft FeOCl-type structure. As J_{nn} is frustrated in the RT phase of 1D antiferromagnetic chains,[1,5] any displacement of a Ti ion away from its RT equilibrium position favors a particular superexchange path resulting in a net energy gain. Given the relatively large value of J_{nn} and its frustrated character, we expect the magnetoelastic energy gain associated with such displacements to yield a rather important contribution to the free energy of the low-temperature phases. We propose that the competition between the two magnetoelastic couplings associated, respectively, with J_b and J_{nn} is at the origin of the complex phase diagram of TiO*X* and in particular of the existence of an incommensurate phase[15,40,41] between the RT phase and the spin-Peierls ground state. The intermediate phase is characterized by the opening of a pseudogap[9,42–44] in the magnetic spectrum, indicative of the formation of a minority of spin-singlets. The most likely scenario for this phase is the coexistence of a minority of spin singlets em-

bedded in a paramagnetic state with antiferromagnetic correlations, which is accompanied by a structural distortion incommensurate with the RT lattice. The formation of a fraction of spin-singlets is accompanied by an overall distortion of the structure, resulting, we argue, in a free energy gain on the remaining uncoupled spins due to the J_{nn} superexchange. The sensitive dependence of the critical temperatures on halide substitution found experimentally may be expected in this case as the size and position of the halide ions influences the overlap between Ti and O states and thereby the magnitude of the magnetoelastic coupling.

Lower values of the transition temperatures (especially T_{c1}) are expected in TiOBr than in TiOCl, as the larger J_{nn}/J_b ratio suggests also a stronger competition between the associated magnetoelastic couplings in the former compound. For the same reason a larger T_{c2}/T_{c1} ratio may be expected in TiOBr. A microscopic investigation of the magnetic ordering in the intermediate phase would be necessary to settle this issue and to understand quantitatively the role played by the interchain superexchange in the TiO*X* system.

IV. CONCLUSIONS

A TiOBr crystalline sample was probed by photoemission and x-ray absorption spectroscopy and theoretical calculations were performed on the electronic and magnetic structure of the room temperature phase. The O 1*s* and Ti 2*p* XAS spectra provide direct experimental evidence for the complete lifting of degeneracy in the Ti 3*d* shell due to the crystal field. The five Ti $3d^1$-derived states may still be grouped roughly into two sets, separated by an average O_h-like crystal field splitting of about 1.6 eV. The computed separation between the ground-state and first-excited $3d^1$ orbital in TiOBr is found to be 0.34 eV, which is too large to give rise to *d*-orbital mixing or ordering.

On the basis of our theoretical results, the first peak in the O 1*s* XAS spectrum is associated with excitations to high valence-spin O $1s^1$ Ti $3d$ $t_{2g}{}^2$-like final states. The second peak has contributions from the same configuration with a low valence-spin value, and from O $1s^1$ Ti $3d$ $t_{2g}{}^1e_g{}^1$-like configurations. A large number of states and the richness of the interactions in TiOBr conspire to give rise to the rich structure observed in the Ti 2*p* XAS spectra.

The observation of absorption at the O 1*s* edge and the resonant enhancement of the lowest binding energy feature as the photon energy varies across the O K edge points to a significant admixture of O 2*p* character in the Ti 3*d* ground state. Such hybridization leads to superexchange interactions between Ti ions on different chains. On the other hand, the absence of absorption from the Br 3*s* and 3*p* core level thresholds confirms that no Br 4*p*-Ti 3*d* mixing is present. Our cluster calculations indicate that the nearest-neighbor interchain interaction J_{nn} is a significant 19% (12%) fraction of the intrachain exchange J_b in TiOBr (TiOCl). This leads one to speculate that the TiO*X* phase diagram results from the competition between the spin-Peierls ordering associated with the exchange along **b** and the magnetoelastic coupling associated to the frustrated superexchange J_{nn} between next-neighbor chains.

ACKNOWLEDGMENTS

R.M. is thankful to M. Mostovoy for an insightful discussion. This work was supported by the Dutch Stichting voor Fundamenteel Onderzoek der Materie (FOM), which is financially supported by the Nederlandse Organisatie voor Wetenschappelijk Onderzoek (NWO). The research of S.v.S. was supported by the German Science Foundation (DFG).

[1] A. Seidel, C. A. Marianetti, F. C. Chou, G. Ceder, and P. A. Lee, Phys. Rev. B **67**, 020405(R) (2003).
[2] H. G. von Schnering, M. Collin, and M. Hassheider, Z. Anorg. Allg. Chem. **387**, 137 (1972).
[3] H. Schäfer, F. Wartenpfuhl, and E. Weise, Z. Anorg. Allg. Chem. **295**, 268 (1958).
[4] T. Saha-Dasgupta, R. Valentí, H. Rosner, and C. Gros, Europhys. Lett. **67**, 63 (2004).
[5] V. Kataev, J. Baier, A. Möller, L. Jongen, G. Meyer, and A. Freimuth, Phys. Rev. B **68**, 140405(R) (2003).
[6] G. Caimi, L. Degiorgi, P. Lemmens, and F. C. Chou, J. Phys.: Condens. Matter **16**, 5583 (2004).
[7] C. Kato, Y. Kobayashi, and M. Sato, J. Phys. Soc. Jpn. **74**, 473 (2005).
[8] P. Lemmens, K. Y. Choi, G. Caimi, L. Degiorgi, N. N. Kovaleva, A. Seidel, and F. C. Chou, Phys. Rev. B **70**, 134429 (2004).
[9] G. Caimi, L. Degiorgi, N. N. Kovaleva, P. Lemmens, and F. C. Chou, Phys. Rev. B **69**, 125108 (2004).
[10] J. Hemberger, M. Hoinkis, M. Klemm, M. Sing, R. Claessen, S. Horn, and A. Loidl, Phys. Rev. B **72**, 012420 (2005).
[11] D. Fausti, T. T. A. Lummen, C. Angelescu, R. Macovez, J. Luzon, R. Broer, P. Rudolf, P. H. M. van Loosdrecht, N. Tristan, B. Büchner, S. van Smaalen, A. Möller, G. Meyer, and T. Taetz, Phys. Rev. B **75**, 245114 (2007).
[12] M. Hoinkis, M. Sing, J. Schäfer, M. Klemm, S. Horn, H. Benthien, E. Jeckelmann, T. Saha-Dasgupta, L. Pisani, R. Valentí, and R. Claessen, Phys. Rev. B **72**, 125127 (2005).
[13] R. Rückamp, J. Baier, M. Kriener, M. W. Haverkort, T. Lorenz, G. S. Uhrig, L. Jongen, A. Möller, G. Meyer, and M. Grüninger, Phys. Rev. Lett. **95**, 097203 (2005).
[14] D. V. Zakharov, J. Deisenhofer, H.-A. Krug von Nidda, P. Lunkenheimer, J. Hemberger, M. Hoinkis, M. Klemm, M. Sing, R. Claessen, M. V. Eremin, S. Horn, and A. Loidl, Phys. Rev. B **73**, 094452 (2006).
[15] A. Krimmel, J. Strempfer, B. Bohnenbuck, B. Keimer, M. Hoinkis, M. Klemm, S. Horn, A. Loidl, M. Sing, R. Claessen, and M. v. Zimmermann, Phys. Rev. B **73**, 172413 (2006).
[16] L. Palatinus, A. Schönleber, and S. van Smaalen, Acta Crystallogr., Sect. C: Cryst. Struct. Commun. **61**, i48 (2005).
[17] R. Denecke, P. Väterleina, M. Bässlera, N. Wassdahla, S. Butorina, A. Nilssona, J.-E. Rubenssona, J. Nordgrena, N. Mårtenssona, and R. Nyholmb, J. Electron Spectrosc. Relat. Phenom. **101**, 971 (1999).
[18] N. W. Winter, R. M. Pitzer, and D. K. Temple, J. Chem. Phys. **86**,

3549 (1987).
[19] R. Pou-Amerigo, M. Merchan, P.-O. Widmark, and B. O. Roos, Theor. Chim. Acta **92**, 149 (1995).
[20] P.-O. Widmark, P.-A. Malmqvist, and B. O. Roos, Theor. Chim. Acta **77**, 291 (1990).
[21] G. Karlström, R. Lindh, P.-A. Malmqvist, B. O. Roos, U. Ryde, V. Veryazov, P.-O. Widmark, M. Cossi, B. Schimmelpfennig, P. Neogrady, and L. Seijo, Comput. Mater. Sci. **28**, 222 (2003).
[22] A. Bergner, M. Dolg, W. Kuechle, H. Stoll, and H. Preuss, Mol. Phys. **80**, 1431 (1993).
[23] The final states with $S=3/2$ are $3\times10=30$ (3 from the $2p$ hole and 10 from the two $3d$ electrons with parallel spins); for $S=1/2$ there are 30 states where the two $3d$ electrons have parallel spins and 45 with antiparallel spins, for a total of 75. The total number of lines in the absorption spectrum is thus $75\times2+30\times4=270$.
[24] J. P. Crocombette and F. Jollet, J. Phys.: Condens. Matter **8**, 5253 (1996).
[25] H. Nagao, M. Nishino, Y. Shigeta, T. Soda, Y. Kitagawa, T. Onishi, Y. Yoshioka, and K. Yamaguchi, Coord. Chem. Rev. **198**, 265 (2000).
[26] A. D. Becke, J. Chem. Phys. **98**, 5648 (1993).
[27] R. Krishnan, J. S. Binkley, R. Seeger, and J. A. Pople, J. Chem. Phys. **72**, 650 (1980).
[28] P. De Boeij (private communication).
[29] M. Hoinkis, M. Sing, S. Glawion, L. Pisani, R. Valenti, S. van Smaalen, M. Klemm, S. Horn, and R. Claessen, Phys. Rev. B **75**, 245124 (2007).
[30] N. V. Smith and F. J. Himpsel, *Handbook on Synchrotron Radiation, Volume 1B*, edited by Ernst-Eckhard Koch (North-Holland, Amsterdam, 1983), Chap. 9.
[31] R. Rückamp, E. Benckiser, M. W. Haverkort, H. Roth, T. Lorenz, A. Freimuth, L. Jongen, A. Möller, G. Meyer, P. Reutler, B. Büchner, A. Revcolevschi, S.-W. Cheong, C. Sekar, G. Krabbes, and M. Grüninger, New J. Phys. **7**, 1367 (2005).
[32] F. M. F. de Groot, M. Grioni, J. C. Fuggle, J. Ghijsen, G. A. Sawatzky, and H. Petersen, Phys. Rev. B **40**, 5715 (1989).
[33] S. Räth, F. Gracia, F. Yubero, J. P. Holgado, A. I. Martin, D. Batchelor, and A. R. González-Elipe, Nucl. Instrum. Methods Phys. Res. B **200**, 248 (2003).
[34] Y. Tanabe and S. Sugano, J. Phys. Soc. Jpn. **9**, 753 (1954); **9**, 766 (1954).
[35] R. D. Leapman and L. A. Grunes, Phys. Rev. Lett. **45**, 397 (1980); R. D. Leapman, L. A. Grunes, and P. L. Fejes, Phys. Rev. B **26**, 614 (1982).
[36] The superexchange along **a** would vanish if the bilayer were not buckled, since in this case the exchange direction would be orthogonal to the $3d$ ground state orbital. This indicates that the magnetic coupling along **a**, originates from the small tilt between the oxygen orbitals involved and stems from mutually orthogonal states at the same oxygen site, which explains its weak ferromagnetic character.
[37] P. Lemmens, K. Y. Choi, R. Valentí, T. Saha-Dasgupta, E. Abel, Y. S. Lee, and F. C. Chou, New J. Phys. **7**, 74 (2005).
[38] I. P. R. Moreira and F. Illas, Phys. Chem. Chem. Phys. **8**, 1645 (2006).
[39] M. Hase, I. Terasaki, and K. Uchinokura, Phys. Rev. Lett. **70**, 3651 (1993).
[40] S. van Smaalen, L. Palatinus, and A. Schönleber, Phys. Rev. B **72**, 020105(R) (2005).
[41] A. Schönleber, S. van Smaalen, and L. Palatinus, Phys. Rev. B **73**, 214410 (2006).
[42] T. Imai and F. C. Chou, arXiv:cond-mat/0301425.
[43] P. J. Baker, S. J. Blundell, F. L. Pratt, T. Lancaster, M. L. Brooks, W. Hayes, M. Isobe, Y. Ueda, M. Hoinkis, M. Sing, M. Klemm, S. Horn, and R. Claessen, Phys. Rev. B **75**, 094404 (2007).
[44] A. Seidel, Ph.D. thesis, Massachusetts Institute of Technology, 2003.